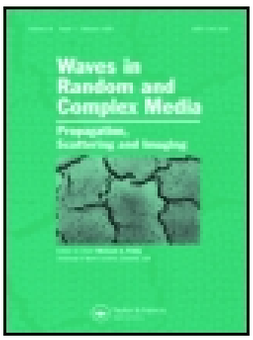

Waves in Random and Complex Media

ISSN: 1745-5030 (Print) 1745-5049 (Online) Journal homepage: http://www.tandfonline.com/loi/twrm20

Stochastic effects on the bistatic transfer function of a planar scatterer distribution

Ignacio Gavier, Damián H. Zanette & Octavio Cabrera

To cite this article: Ignacio Gavier, Damián H. Zanette & Octavio Cabrera (2018): Stochastic effects on the bistatic transfer function of a planar scatterer distribution, Waves in Random and Complex Media, DOI: 10.1080/17455030.2018.1551643

To link to this article: https://doi.org/10.1080/17455030.2018.1551643

Published online: 03 Dec 2018.

WAVES IN RANDOM AND COMPLEX MEDIA
https://doi.org/10.1080/17455030.2018.1551643

Taylor & Francis
Taylor & Francis Group

Stochastic effects on the bistatic transfer function of a planar scatterer distribution

Ignacio Gavier, Damián H. Zanette and Octavio Cabrera

Centro Atómico Bariloche and Instituto Balseiro, Comisión Nacional de Energía Atómica and Universidad Nacional de Cuyo, Consejo Nacional de Investigaciones Científicas y Técnicas, San Carlos de Bariloche, Argentina

ABSTRACT

We evaluate the effects of several stochastic factors on signal transmission through a planar distribution of stationary scatterers, with non-collocated transmitter and receiver (bistatic configuration). The transmission channel is described by means of its transfer function, which –as a result of randomness in the scatterer distribution– fluctuates around its expectation value. Specifically, we consider randomness in the scatterer positions (both on the plane and in height), in their radar cross sections, and in the scattering phases. Our analytical results provide a quantitative relation between the parameters that characterize random components of each kind, and the fluctuations that alter the transfer function.

ARTICLE HISTORY
Received 15 May 2018
Accepted 17 November 2018

KEYWORDS
Bistatic radar; channel models; transfer function; radar clutter

1. Introduction

Bistatic radars are based on the detection of signals which are not emitted at the same place where they are received. This kind of geometric configuration, where the distance between transmitter and receiver is comparable to the distance to the target [1], has several advantages over its monostatic counterpart with collocated transmitter and receiver. Among them, an enhanced resolution and signal information contents [2], the possibility of exploiting third party transmitters [3], and strategic benefits such as covert operation of inexpensive and mobile receivers [4], are worth mentioning. Synthetic aperture radars (SAR), which are among the most up-to-date remote sensing systems in scientific applications [5–8], are designed on the basis of bistatic configurations. This is also the case of passive radars, where sensing is implemented using non-cooperative transmitters, thus reducing manufacturing and operational costs [9]. Forward-scattering radars are another member of the same class [10].

Target detection and characterization with radars are based on the comparison of emitted and received signals. Differences between these signals bear information on how the environment affects the original emission by adding reflections at material objects, thus making it possible to infer data on the location, motion, and nature of the scatterers. The construction of models for the transmission channel embodied by the environment is a

CONTACT Damián H. Zanette zanette@cab.cnea.gov.ar

crucial step in the interpretation of the information derived from radar measurements, and therefore constitutes a basic ingredient of signal processing. Well-known statistical models for radar cross-section distributions –e.g. Rayleigh, Rician, Weibull [11]– as well as standard propagation models –e.g. Okumura-Hata [12], and the recommendations of the International Telecommunication Union (ITU-R)– are examples based on both heuristic arguments and empirical results.

On the other hand, *ab initio* computation of the effects of the environment on signal propagation –although necessarily restricted to stylized representations of the distribution and the nature of scatterers– can be used as a starting point for the construction of more refined models, overcoming the phenomenological essence of the standard descriptions mentioned above. In a recent contribution [13], we have presented analytical results characterizing the transmission channel formed by a planar distribution of point scatterers, within a bistatic configuration. Our characterization was based on the computation of the transfer function, which measures the ratio between the received signal and the transmitted signal for each frequency component –i.e. in the Fourier representation.

The first step in the present paper consists in removing various assumptions and constraints on the scattering models studied in our previous contribution. However, the main focus is put on analyzing the effect of several kinds of stochastic factors, expected to be present in any real distribution of environmental scatterers. Specifically, we consider random components in the position of the scatterers, in their radar cross sections, in the phase shifts due to scattering, and in the height of scatterers above or below the reference plane. The main goal consists in quantitatively relating the parameters which specify the strength of randomness, to the fluctuations that these random components induce in the transfer function. Our methodology and results provide tools for evaluating the effects of several sources of clutter on the received signal of radars, and other sensing and communication systems based on bistatic configurations [14–16].

2. Bistatic transfer function

We consider a transmitter at position $\mathbf{r}_T$, emitting a signal of amplitude $T(t)$, and a receiver at position $\mathbf{r}_R$. Both transmitter and receiver are stationary and isotropic. Assuming that propagation occurs in free space in the presence of N stationary non-interacting point scatterers, the amplitude of the received signal reads

$$R(t) = \frac{1}{d_0} T(t - t_0) + \sum_{k=1}^{N} \frac{\sqrt{\sigma_k}}{d_T^{(k)} d_R^{(k)}} T(t - t_k), \tag{1}$$

where $d_0 = |\mathbf{r}_R - \mathbf{r}_T|$ is the distance between transmitter and receiver, and $d_T^{(k)} = |\mathbf{r}_k - \mathbf{r}_T|$ and $d_R^{(k)} = |\mathbf{r}_k - \mathbf{r}_R|$ are the distances from the kth scatterer, situated at position $\mathbf{r}_k$, to the transmitter and the receiver, respectively. Figure 1(a) illustrates these definitions. The delay time from transmitter to receiver is $t_0 = d_0/c$, and $t_k = (d_T^{(k)} + d_R^{(k)})/c$ is the total delay of the echo received from the kth scatterer. The factor $\sqrt{\sigma_k}$ is the square root of the corresponding radar cross section (RCS). In the frequency domain, Equation (1) reads

$$\tilde{R}(\omega) = \frac{1}{d_0} \tilde{T}(\omega) \left[1 + \tau(\omega)\right] \exp\left(-i \frac{\omega d_0}{c}\right), \tag{2}$$

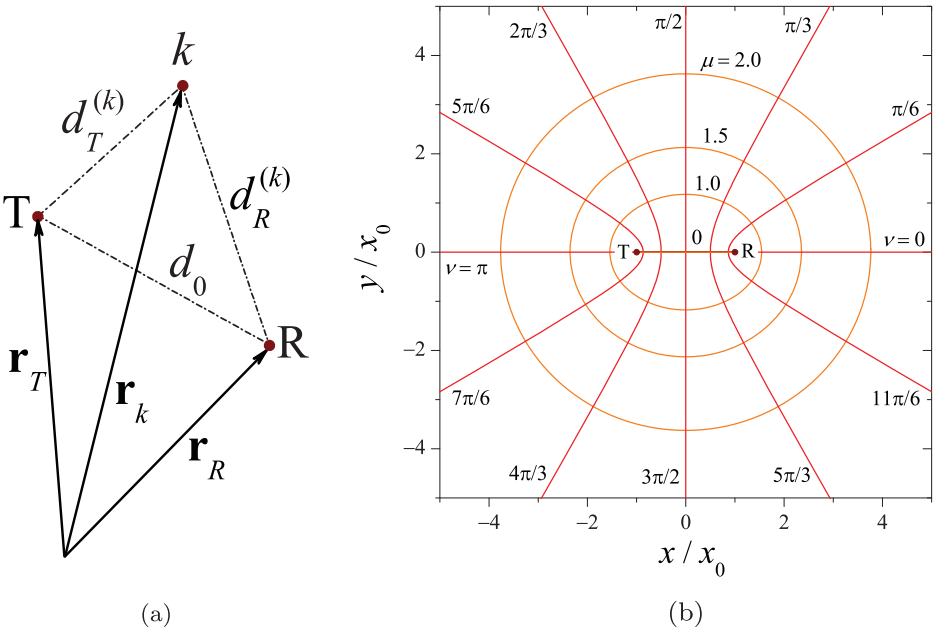

Figure 1. Positions, distances, and the setup of elliptic coordinates in the bistatic geometric configuration. (a) Notation for positions and mutual distances between the transmitter (T), receiver (R), and scatterer k (b) Curves of constant μ or ν in the elliptic coordinate system. The Cartesian coordinates are normalized by the distance x_0 between the origin and the foci, represented as dots (T: transmitter, R: receiver).

where tildes denote Fourier transforms. The quantity

$$\tau(\omega) = \sum_{k=1}^{N} \mathcal{T}(\mathbf{r}_k, \omega) \tag{3}$$

is the *transfer function* of the scattering channel, with

$$\mathcal{T}(\mathbf{r}_k, \omega) = \frac{d_0}{d_T^{(k)} d_R^{(k)}} \sqrt{\sigma_k} \exp\left[i \frac{\omega}{c} \left(d_0 - d_T^{(k)} - d_R^{(k)} \right) \right] \tag{4}$$

the contribution of the scatterer situated at $\mathbf{r}_k$.

Being a frequency-by-frequency description of the scattering channel, the transfer function can be immediately extended to take into account a dependence on frequency in the RCS, as well as a frequency-dependent phase shift during signal reflection at each scatterer (none of them considered in Ref. [12]). In fact, replacing

$$\sqrt{\sigma_k} \to \chi_k(\omega) \equiv \xi_k(\omega) \exp[i\phi_k(\omega)] \tag{5}$$

in Equation (4), we add a dependence on ω to the RCS, now given by $\sigma_k(\omega) = \xi_k(\omega)^2$, and a phase shift $\phi_k(\omega)$.

Assume now that the positions $\mathbf{r}_k$ of the scatterers, together with those of transmitter and receiver, $\mathbf{r}_T$ and $\mathbf{r}_R$, are all coplanar. Introducing a suitably defined distribution over the

plane, the transfer function (3) can be expressed as the integral

$$\tau(\omega) = d_0 \exp\left(i\frac{\omega d_0}{c}\right) \int \rho(\mathbf{r},\omega) \frac{\exp[-i\omega(|\mathbf{r}-\mathbf{r}_T| + |\mathbf{r}-\mathbf{r}_R|)/c]}{|\mathbf{r}-\mathbf{r}_T||\mathbf{r}-\mathbf{r}_R|}\, \mathrm{d}^2\mathbf{r}, \tag{6}$$

where $\rho(\mathbf{r},\omega)\,\mathrm{d}^2\mathbf{r} = \chi(\mathbf{r},\omega)n(\mathbf{r})\,\mathrm{d}^2\mathbf{r}$ is the number of scatterers $n(\mathbf{r})\,\mathrm{d}^2\mathbf{r}$ inside the surface element $\mathrm{d}^2\mathbf{r}$ at position $\mathbf{r}$, weighted by the corresponding value of $\chi(\mathbf{r},\omega)$. This integral adopts a particularly simple form when expressed in elliptic coordinates with foci at the positions of transmitter and receiver (see Appendix). In fact, except for the density $\rho(\mathbf{r},\omega)$, the integrand is independent of the elliptic 'angle' ν, and depends on the 'modulus' μ only. Figure 1(b) shows curves of constant μ or ν over the plane. In elliptic coordinates, Equation (6) reads

$$\tau(\omega) = d_0 \int_0^\infty \bar{\rho}(\mu,\omega) \exp\left[i\frac{\omega d_0}{c}(1-\cosh\mu)\right] \mathrm{d}\mu, \tag{7}$$

with $\bar{\rho}(\mu,\omega) = \int_0^{2\pi} \rho(\mathbf{r},\omega)\,\mathrm{d}\nu$. The product $\bar{\rho}(\mu,\omega)\,\mathrm{d}\mu$ encompasses the contribution to the transfer function coming from the scatterers along the ellipse of 'modulus' μ and width $\mathrm{d}\mu$, irrespectively of their 'angle' ν. The integral in Equation (7) can be exactly computed for selected scatterer distributions, yielding explicit expressions for $\tau(\omega)$. Moreover, when $\bar{\rho}$ does not depend on the frequency, the limits of large and small ω can be given as asymptotic expansions, and the inverse problem of finding $\bar{\rho}(\mu)$ as a function of $\tau(\omega)$ is exactly solvable [13].

For the sake of concreteness, in the following we focus the attention on elliptically 'isotropic' scatterer distributions, for which the scatterer number density can be written as

$$n(\mathbf{r})\,\mathrm{d}^2\mathbf{r} \equiv \frac{N}{2\pi}\eta(\mu)\,\mathrm{d}\mu\,\mathrm{d}\nu. \tag{8}$$

Here, the density profile over the ellipse 'modulus', $\eta(\mu)$, satisfies $\int_0^\infty \eta(\mu)\,\mathrm{d}\mu = 1$. If we further assume that the frequency dependence of both the RCS and the scattering phase shift is statistically uncorrelated with the scatterer positions, so that $\chi(\mathbf{r},\omega) \equiv \chi_0(\omega) = \xi_0(\omega)\exp[i\phi_0(\omega)]$ for all $\mathbf{r}$, the transfer function becomes

$$\tau(\omega) = \frac{4N\chi_0(\omega)}{d_0} \int_0^\infty \eta(\mu) \frac{\exp[i\omega d_0(1-\cosh\mu)/c]}{\cosh\mu\sinh\mu}\,\mathrm{d}\mu. \tag{9}$$

Due to the fast decay of the integrand as $\mu \to \infty$ –and disregarding possible non-integrable singularities of $\eta(\mu)$ for intermediate values of the variable– the only condition for the convergence of the integral in Equation (9) is that, for $\mu \to 0$, $\eta(\mu)$ vanishes at least as fast as μ^ϵ for some $\epsilon > 0$. In practice, this condition prevents considering any distribution with a finite density of scatterers on the segment between transmitter and receiver. Scatterers asymptotically close to transmitter or receiver, in particular, provide divergently large contributions to $\tau(\omega)$.

In the next section, we study how the transfer function responds to several stochastic features in the scatterer properties, which add different forms of clutter to the bistatic transmission channel.

3. Effects of randomness

In this section, we study how the transfer function responds to several stochastic factors associated with the spatial distribution and physical properties of scatterers. Specifically, we consider the effects of randomness in the scatterer positions over the plane, in their RCS, and in the signal phase shifts during reflections. Finally, we relax the assumption of a planar scatterer distribution, and study the effect of (small) random displacements with respect to a reference plane. In all cases, our approach is the same. Starting from Equation (3), we compute the expectation value and the variance induced by stochasticity on the transfer function. Then, much as for Equations (6) to (9), we provide integral expressions, where stochastic effects are mathematically more explicit.

3.1. Randomness in the scatterer positions

For any given scatterer density $n(\mathbf{r})$, local irregularities in the distribution of the N scatterers determine that the transfer function calculated from (3) differs from the result of (7). The same kind of difference arises if the integral in Equation (7) is calculated using a Monte Carlo algorithm, sampling the integrand at N randomly selected points on the plane. Thus, the first stochastic effect that we consider here concerns the fluctuations in the value of the transfer function over different realizations of the scatterer positions for a prescribed form of $n(\mathbf{r})$. To isolate this specific effect, we assume that $\chi_k(\omega)$ is the same for all scatterers: $\chi_k(\omega) = \xi_0(\omega)\exp[i\phi_0(\omega)] \equiv \chi_0(\omega)$ for all k (as in Marcum RCS model [11]).

When the position of a scatterer is randomly sorted following the density $n(\mathbf{r})$, the probability that it lies inside a small area δA_j around position $\mathbf{r}_j$ is $p_j(\mathbf{r}) = n(\mathbf{r}_j)\delta A_j/N$. The number of scatterers N_j in δA_j, in turn, obeys a multinomial distribution [17]. Its expectation value is $\mathrm{E}[N_j] = Np_j$, while its autocorrelation reads $\mathrm{E}[N_jN_{j'}] = Np_j[\delta_{jj'} + (N-1)p_{j'}]$, with $\delta_{jj'}$ the Kronecker delta. The resulting expectation and autocorrelation for the transfer function, calculated from Equation (3), are given by

$$\begin{aligned}\mathrm{E}[\tau(\omega)] &= \sum_j \mathrm{E}[N_j]\mathcal{T}(\mathbf{r}_j,\omega),\\ \mathrm{E}[\tau(\omega_1)\tau^*(\omega_2)] &= \sum_{jj'} \mathrm{E}[N_jN_{j'}]\mathcal{T}(\mathbf{r}_j,\omega_1)\mathcal{T}^*(\mathbf{r}_{j'},\omega_2),\end{aligned} \tag{10}$$

where the sums run over all the areas δA_j, covering the whole plane, and the asterisk indicates complex conjugate.

In the limit where the areas δA_j are infinitesimal, the sums over surface elements transform into integrals. In particular, the expectation[1] $\mathrm{E}[\tau]$ becomes identical to the integral in Equation (7), indicating that the average value of $\tau(\omega)$ over random realizations of the scatterer positions coincides with the transfer function calculated over the continuous distribution $n(\mathbf{r})$. For the isotropic densities defined by Equation (8), the expectation of the transfer function reduces to the expression given in Equation (9).

In turn, evaluating the autocorrelation for $\omega_1 = \omega_2$, we calculate the variance of the transfer function, $\mathrm{Var}[\tau] = \mathrm{E}[|\tau|^2] - |\mathrm{E}[\tau]|^2$, which for isotropic densities yields

$$\mathrm{Var}[\tau(\omega)] = \frac{8N\xi_0(\omega)^2}{d_0^2}\int_0^\infty \eta(\mu)\frac{2\cosh^2\mu - 1}{\cosh^3\mu\sinh^3\mu}\,\mathrm{d}\mu. \tag{11}$$

Note that Var$[\tau]$ depends on ω through the coefficient $\xi_0(\omega)^2$ only. Because both E$[\tau]$ and Var$[\tau]$ are proportional to the number of scatterers N, relative fluctuations in the transfer function, as measured by the coefficient of variation

$$V_\tau = \frac{\sqrt{\text{Var}[\tau(\omega)]}}{|\text{E}[\tau(\omega)]|}, \tag{12}$$

decrease as N grows: $V_\tau \sim 1/\sqrt{N}$. In contrast with the integral in Equation (9), convergence in Equation (11) requires that, for $\mu \to 0$, $\eta(\mu)$ vanishes at least as fast as $\mu^{2+\epsilon}$ for some $\epsilon > 0$. This stronger condition indicates that the divergent contribution of scatterers near the transmitter and the received has a larger effect on the variance of $\tau(\omega)$.

In order to compare with our analytical results, we have measured the standard deviation SD$[\tau] = \sqrt{\text{Var}[\tau]}$, for several frequencies, over sets of 300 realizations of the scatterer distribution. The transfer function $\tau(\omega)$ was calculated by numerical evaluation of the sum in Equation (3), with N varying from 100 to 10^6. We sorted the scatterer positions from a class of isotropic distributions with $\eta(\mu) \equiv \eta_{a,b}(\mu) = C_{a,b} \exp(-\cosh\mu) \sinh^a \mu \cosh^b \mu$, where $C_{a,b}$ is a suitable normalization constant, for four combinations of the exponents a and b. Due to the proportionality to $\exp(-\cosh\mu)$, these distributions correspond to scatterer densities which decay exponentially for large distances from transmitter and receiver. Their detailed behavior for short distances –and, in particular, their integrability in Equation (11)– depends on a and b. For selected values of the exponents, moreover, Var$[\tau(\omega)]$ can be exactly evaluated. Regarding the RCS, we have taken $\xi_0(\omega) = 10^{-3} d_0$ for all ω. With this choice, according to Equation (11), we expect that Var$[\tau(\omega)]$ is independent of the frequency.

Symbols in Figure 2 stand for numerical results. For the three lowermost sets, full lines correspond to the analytical result for $\sqrt{\text{Var}[\tau]}$. We find an excellent agreement, especially for large frequencies. For the uppermost set, on the other hand, the integral in Equation (11) does not converge. In this case, SD$[\tau]$ grows faster than $\sqrt{N}$, as demonstrated by the dashed line. On the other hand, its independence of the frequency is preserved.

3.2. Randomness in the radar cross section (RCS)

The second stochastic effect that we consider here is due to statistical variations in the value of the RCS between scatterers. To this end, we write the square root of the RCS of scatterer k as

$$\xi_k(\omega) = \xi_0(\omega) + g[\xi_0(\omega)] W_k, \tag{13}$$

where W_k is a non-dimensional stochastic variable with zero mean and delta-like autocorrelation: E$[W_k W_{k'}] = \delta_{kk'}$. In order to isolate the effect, we assume that all the phases $\phi_k(\omega)$ in Equation (5) are identical. The expectation and the autocorrelation of ξ_k over the set of all scatterers are

$$\text{E}[\xi_k] = \xi_0, \quad \text{E}[\xi_k \xi_{k'}] = \xi_0^2 + g(\xi_0)^2 \delta_{kk'}, \tag{14}$$

respectively. The function $g(\xi_0)$, which weights the standard deviation of ξ_k, is introduced to take into account that in statistical models for cross section distributions (e.g. Rayleigh, 4th-degree chi-square, Rice, Weibull, among others [11]) the RCS mean value and variance depend –at least, partially– on each other, via the parameters that define each distribution.

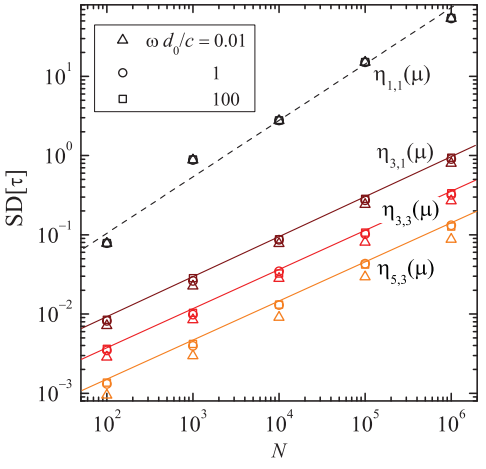

Figure 2. Standard deviation of the transfer function, SD[τ], as a function of the number of scatterers, N, for isotropic distributions with $\eta_{a,b}(\mu) = C_{a,b} \exp(-\cosh \mu) \sinh^a \mu \cosh^b \mu$, for four combinations of the exponents a and b. Different symbols stand for numerical results at three frequencies, as indicated in the label. Full lines for the three lowermost sets are analytical results. For the uppermost set, the dashed line is a guide to the eye.

Replacing Equation (13) into Equation (3) and averaging over the stochastic variable W_k, we can calculate the expectation values $\mathrm{E}[\tau(\omega)]$ and $\mathrm{E}[\tau(\omega_1)\tau^*(\omega_2)]$ by summing over individual scatterers. When the sums are approximated by integrals, $\mathrm{E}[\tau(\omega)]$ coincides (as in Section 3.1) with the value of $\tau(\omega)$ obtained for uniform $\chi_k(\omega)$. For isotropic densities, $\mathrm{E}[\tau(\omega)]$ is identical to the expression in Equation (9). Similarly, the variance differs from the result given in Equation (11) just by a multiplicative coefficient which determines its dependence on the frequency:

$$\mathrm{Var}[\tau(\omega)] = \frac{8Ng(\xi_0)^2}{d_0^2} \int_0^\infty \eta(\mu) \frac{2\cosh^2 \mu - 1}{\cosh^3 \mu \sinh^3 \mu} \, \mathrm{d}\mu. \tag{15}$$

As in the case of random scatterer positions, the coefficient of variation of Equation (12) decays here with the number of scatterers as $V_\tau \sim 1/\sqrt{N}$. This behavior is now due to local self-averaging of the stochastic distribution of RCS, within any given spatial domain, as the number of scatterers grows.

Symbols in Figure 3 show the standard deviation of the transfer function versus the standard deviation of the RCS square root obtained from numerical computation of the sum in Equation (3), for $N = 10^6$ scatterers and $\xi_0 = 10^{-3} d_0$ for all ω, over 300 realizations of their RCS. Cross sections were drawn from a triangular distribution of unitary mean value and several widths. We considered three of the isotropic distributions introduced in Section 3.1, and computed the transfer function for three frequencies. The agreement with the theoretical prediction, represented by lines, is again excellent.

3.3. *Randomness in the scattering phase*

When, at each scatterer k, the signal is shifted in phase by a random amount, we expect that the received signal is degraded by interference between reflections at mutually close

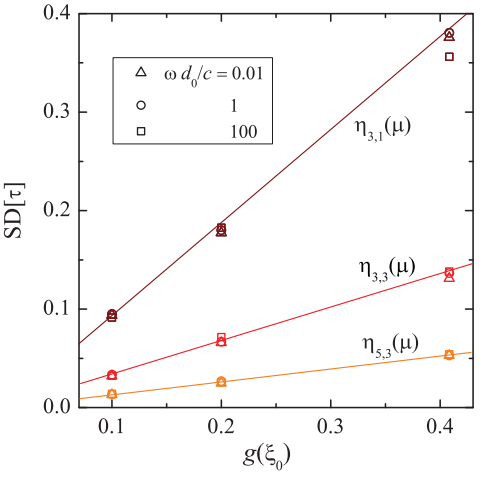

Figure 3. Standard deviation of the transfer function, SD[τ], as a function of the standard deviation of the RCS square root, $g(\xi_0)$, for three of the isotropic distributions $\eta_{a,b}(\mu)$ considered in Figure 2. Symbols stand for numerical results at three frequencies, and lines correspond to analytical results.

scatterers, with a resulting decrease in the transfer function. We write the phase change at each reflection as

$$\phi_k(\omega) = \phi_0(\omega) + \Delta_k(\omega), \tag{16}$$

where the random phases $\Delta_k(\omega)$ are drawn from a specified distribution $f(\Delta, \omega)$. To isolate this effect, moreover, we take the same RCS for all oscillators. In other words, $\chi_k(\omega) = \xi_0(\omega)\exp[i\phi_0(\omega) + i\Delta_k(\omega)] \equiv \chi_0(\omega)\exp[i\Delta_k(\omega)]$. The explicit specification of the distribution $f(\Delta, \omega)$ is here necessary because of the nonlinear dependence of the transfer function on the phase shifts $\phi_k(\omega)$. For instance, the expectation $\mathrm{E}[\tau(\omega)]$ is proportional to $\mathrm{E}[\exp(i\Delta_k)] = \mathrm{E}[\cos\Delta_k] + i\,\mathrm{E}[\sin\Delta_k]$, whose calculation explicitly involves $f(\Delta, \omega)$. This contrast with the linear dependence on the square root of the RCS, where the specification of the mean value and standard deviation of $\xi_k(\omega)$ –cf. Equation (13)– suffices to calculate the homologous quantities for $\tau(\omega)$, as done in Section 3.2.

For isotropic densities, the expectation of the transfer function turns out to be

$$\mathrm{E}[\tau(\omega)] = \frac{4N\chi_0(\omega)}{d_0}\mathrm{E}[\exp(i\Delta_k)]\int_0^\infty \eta(\mu)\frac{\exp[i\omega d_0(1-\cosh\mu)/c]}{\cosh\mu\,\sinh\mu}\,\mathrm{d}\mu. \tag{17}$$

For instance, choosing a Gaussian distribution with frequency-dependent standard deviation $\Sigma(\omega)$,

$$f(\Delta, \omega) = \frac{1}{\sqrt{2\pi\,\Sigma(\omega)^2}}\exp\left[-\frac{\Delta^2}{2\Sigma(\omega)^2}\right], \tag{18}$$

we find $\mathrm{E}[\exp(i\Delta_k)] = \exp[-\Sigma(\omega)^2/2]$. Thus, $\mathrm{E}[\tau(\omega)]$ is modified by the phase shift distribution through the coefficient $\exp[-\Sigma(\omega)^2/2] < 1$. This factor represents a reduction in the transfer function due to the increasing incoherence between local reflections of the transmitted signal, as the dispersion in the random phase shifts grows.

It can be shown that the reduction of the transfer function due to randomness in the reflection phases, illustrated above for a Gaussian distribution, occurs for any distribution

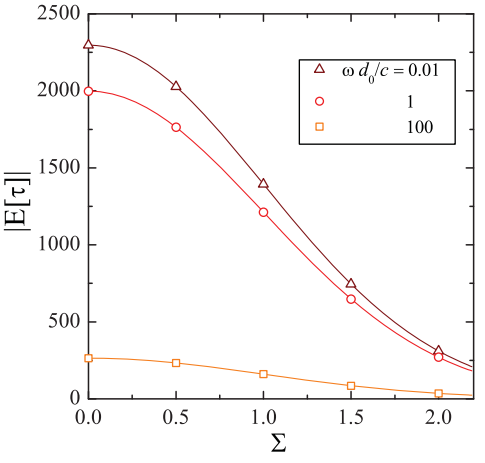

Figure 4. Modulus of the transfer function expectation with a Gaussian distribution of scattering phases, as a function of the standard deviation, for three values of the frequency and an isotropic scatterer distribution given by $\eta_{1,1}(\mu)$ (see Figure 2). Symbols represent results of numerical simulations, and curves stand for analytical results.

$f(\Delta,\omega)$. This is a direct consequence of the mathematical fact that $|\mathrm{E}[\exp(i\Delta_k)]| < 1$, independently of how Δ_k is distributed –except when all the Δ_k are mutually identical, in which case $|\mathrm{E}[\exp(i\Delta_k)]| = 1$. Moreover, assuming that phase shifts are uncorrelated between scatterers, we find that $\mathrm{E}[\exp(i\Delta_k)\exp(i\Delta_{k'})] = |\mathrm{E}[\exp(i\Delta_k)]|^2 + \delta_{kk'}(1 - |\mathrm{E}[\exp(i\Delta_k)]|^2)$ for any distribution. For the transfer function, the resulting variance is

$$\mathrm{Var}[\tau(\omega)] = \frac{8N\xi_0(\omega)^2}{d_0^2}\left(1 - |\mathrm{E}[\exp(i\Delta_k)]|^2\right)\int_0^\infty \eta(\mu)\frac{2\cosh^2\mu - 1}{\cosh^3\mu\sinh^3\mu}\,\mathrm{d}\mu. \tag{19}$$

Note that, as expected, $\mathrm{Var}[\tau]$ vanishes if all phase shifts are identical.

In Figure 4, symbols represent numerical results for the transfer function expectation (in modulus) calculated from Equation (3), with a distribution of scattering phases given by Equation (18), as a function of the standard deviation Σ. Calculations were performed with $N = 10^6$ scatterers, $\xi_0 = 10^{-3}d_0$ for all ω, over 300 realizations for each value of Σ and of the frequency. The scatterer density was $\eta_{1,1}(\mu) = C_{1,1}\exp(-\cosh\mu)\sinh\mu\cosh\mu$ (see Section 3.1). Curves stand for the analytical prediction, Equation (17).

3.4. Randomness in the scatterer heights

Finally, we relax the assumption of a strictly planar distribution of scatterers, by allowing each scatterer k to be located at a random height z_k from the reference (horizontal) plane that contains the transmitter and the receiver. For displacements toward both sides of the reference plane, the distances from scatterer k to transmitter and receiver grow to

$$d_{T,R}^{(k)} = \hat{d}_{T,R}^{(k)}\sqrt{1 + \left(\frac{z_k}{\hat{d}_{T,R}^{(k)}}\right)^2} > \hat{d}_{T,R}^{(k)}, \tag{20}$$

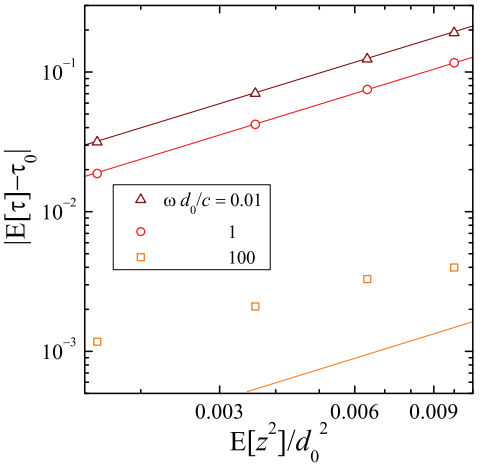

Figure 5. Modulus of the difference between the expectation $E[\tau]$ and the transfer function for a planar distribution, as a function of the variance in the scatterer heights, for three values of the frequency and an isotropic scatterer distribution given by $\eta_{5,3}(\mu)$ (see Figure 2). Symbols stand for results of numerical simulations, and lines correspond to analytical results.

with $\hat{d}_{T,R}^{(k)}$ the corresponding distances if the scatterer were on the plane ($z_k = 0$). Therefore, even if the average displacement is zero, $E[z_k] = 0$, the change of the contributions $\mathcal{T}(\mathbf{r}_k, \omega)$ have the same sign for all scatterers, both in modulus and phase. This implies that, in contrast with the cases of randomness in the scatterer positions and of random RCS (Sections 3.1 and 3.2), stochastic deviations from the reference plane will directly affect the expectation of the transfer function.

An explicit form for $E[\tau]$ can be obtained assuming that the displacements z_k are small as compared with the distances $\hat{d}_{T,R}^{(k)}$, so that $d_{T,R}^{(k)}$ can be approximated by a power series around $\hat{d}_{T,R}^{(k)}$. For isotropic scatterer densities with $\chi_k(\omega) = \chi_0(\omega)$ for all k, and $E[z_k] = 0$, we find, to the first significant order,

$$E[\tau(\omega)] = \tau_0(\omega) - \frac{E[z_k^2]}{d_0^2}\frac{4N\chi_0(\omega)}{d_0}\int_0^\infty \eta(\mu)\frac{\exp[i\omega d_0(1-\cosh\mu)/c]}{\cosh\mu\sinh\mu} \times \left(\frac{1-2\cosh^2\mu+4\cosh^4\mu}{\cosh^2\mu\sinh^4\mu} + i\frac{\omega d_0}{c}\frac{2\cosh^2\mu-1}{\cosh\mu\sinh^2\mu}\right)\mathrm{d}\mu, \tag{21}$$

where $\tau_0(\omega)$ denotes the transfer function for the corresponding planar distribution ($z_k = 0$ for all k), given by the right-hand side of Equation (9). The change in the transfer function turns out to be quadratic in the height displacements compared with d_0, as given by the ratio $E[z_k^2]/d_0^2$. Note, however, that the imaginary part of the quantity in the second line of Equation (21) depends also on the frequency. The truncation of the power series yields a good approximation as long as $\omega d_0/c \lesssim 1$.

A comparison between analytical and numerical results is shown in Figure 5, for $N = 10^6$, $\xi_0 = 10^{-3}$ for all ω, and the isotropic scattering distribution $\eta_{5,3}(\mu)$ (see Section 3.1). As expected, a substantial deviation becomes apparent for sufficiently large frequencies.

4. Conclusion

We have here quantified the effects of several stochastic factors on bistatic signal transmission through a planar distribution of non-interacting point scatterers. With respect to our previous contribution [13], the formulation is now generalized to consider frequency-dependent radar cross sections and phase changes in reflection events.

Stochastic ingredients in the scatterer distribution are a source of clutter affecting transmission, which we have characterized by estimating the fluctuations induced in the transfer function of the corresponding channel. It is useful to summarize the main results as follows.

- Randomness in the positions of the N scatterers with respect to a reference continuous distribution does not affect the expectation of the transfer function. Its fluctuations relative to the expectation, as given by the coefficient of variation, are of order $1/\sqrt{N}$.
- Randomness in the radar cross sections also does not affect the expectation. Fluctuations in the transfer function are proportional to the standard deviation of the cross sections.
- Randomness in the scattering phase shifts determines a reduction of the transfer function expectation, whose detailed form depends on the phase shift distribution.
- Randomness in the scatterer heights with respect to the reference plane modifies the transfer function expectation in an amount which, to the first approximation order, is proportional to the variance of heights and has an imaginary part proportional to the frequency.

For the sake of analysis, the effects of these stochastic factors have been characterized in mutual isolation. However, if they are assumed to be statistically independent of each other, the effects on the transfer function expectation and variance can be added up straightforwardly, making it possible to evaluate their joint outcome when two or more of them are simultaneously present.

Naturally, the four stochastic ingredients considered here do not exhaust all the possible sources of environmental randomness affecting the transfer function. However, our results demonstrate that the present mathematical approach can be employed to deal with a variety of both deterministic and stochastic contributions to signal transmission. The same kind of method can be used to compute other quantities related to signal propagation, such as cross-correlations and power spectral densities. A near-future challenge is to adapt this methodology to consider mobile scatterers, which are dominant in some environments [5, 14, 18], extending the analytical calculation to bistatic ambiguity functions [1].

Note

1. In the following, as done here, we often omit explicit indication of the dependence on ω, for clarity in the notation.

Disclosure statement

No potential conflict of interest was reported by the authors.

ORCID

Damián H. Zanette http://orcid.org/0000-0003-0681-0592

References

[1] Willis NJ, Griffiths HD. Advances in bistatic radar. Raleigh (NC): SciTech Publishing; 2007.
[2] Walterscheid I, Ender JHG, Brenner AR, et al. Bistatic SAR processing and experiments. IEEE Trans Geosci Remote Sens. 2006 Oct;44:2710–2717.
[3] Howland PE, Maksimiuk D, Reitsma G. FM radio based bistatic radar. IEEE Proc Radar Sonar Navig. 2005 Jun;152:107–115.
[4] Olsen KE, Åsen W. Bridging the gap between civilian and military passive radar. IEEE Aero El Sys Mag. 2017 Feb;32:4–10.
[5] Xu ZW, Wu J, Wu ZS. A survey of ionospheric effects on space-based radar. Waves Random Complex Media. 2006;14:S189–S273.
[6] Qazi WA, Emery WJ, Fox-Kemper B. Computing ocean surface currents over the coastal California current system using 30-min-lag sequential SAR Images. IEEE Trans Geosci Remote Sens. 2014 Dec;52:7559–7580.
[7] Iglesias R, Aguasca A, Fabregas X, et al. Ground-based polarimetric SAR interferometry for the monitoring of terrain displacement. IEEE J Sel Top Appl Earth Obs. 2015 Mar;8:980–993.
[8] Monti-Guarnieri A, Broquetas A, Recchia A, et al. Advanced radar geosynchronous observation system: ARGOS. IEEE Geosci Remote Sens Lett. 2015 Jul;12:1406–1410.
[9] Griffiths H, Baker C. Passive bistatic radar. In: Melvin WL, Scheer JA, editors. Principles of modern radar. Vol. III, Radar applications. Edison (NJ): SciTech Publishing; 2014. p. 499–541.
[10] Suberviola I, Mayordomo I, Mendizabal J. Experimental results of air target detection with a GPS forward-scattering radar. IEEE Geosci Remote Sens Lett. 2012 Jan;9:47–51.
[11] Richards MA. Fundamentals of radar signal processing. New York (NY): McGraw-Hill; 2005.
[12] Goldsmith A. Wireless communications. Cambridge (UK): Cambridge University Press; 2005.
[13] Cabrera O, Zanette DH. Bistatic transfer function for a planar distribution of stationary scatterers: analytical results. IEEE Geosci Remote Sens Lett. 2015 Nov;12:2326–2330.
[14] Awada A, Ayari MY, Khenchaf A, et al. Bistatic scattering from an anisotropic sea surface: Numerical comparison between the first-order SSA and the TSM models. Waves Random Complex Media. 2007;16:383–394.
[15] Du Y. A new bistatic model for electromagnetic scattering from randomly rough surfaces. Waves Random Complex Media. 2008;18:109–128.
[16] Voronovich AG, Zavorotny VU. Determination of surface reflectivity using radio signals of opportunity. Waves Random Complex Media. 2016;27:395–402.
[17] Evans M, Hastings N, Peacock B. Statistical distributions. New York (NY): Wiley; 2000.
[18] Xing J, Datta-Barua S, Garrison S, et al. Relative ionospheric ranging delay in LEO GNSS oceanic reflections. IEEE Geosci Remote Sens Lett. 2015 Jul;12:1416–1420.

Appendix. Basic properties of elliptic coordinates

Elliptic coordinates (μ, ν) constitute a planar coordinate system defined with respect to two foci which, in a Cartesian system (x,y), are conventionally situated over the x-axis, at the points $(-x_0, 0)$ and $(+x_0, 0)$. The transformation from elliptic to Cartesian coordinates is given by

$$x = x_0 \cosh\mu \cos\nu, \quad y = x_0 \sinh\mu \sin\nu, \tag{A1}$$

with $0 \leq \mu < \infty$ and $0 \leq \nu < 2\pi$. The inverse transformation can be obtained from the following relations:

$$\cosh\mu = \sqrt{\frac{x^2+y^2+x_0^2}{2x_0^2} + \sqrt{\left(\frac{x^2+y^2-x_0^2}{2x_0^2}\right)^2 + \left(\frac{y}{x_0}\right)^2}}, \tag{A2}$$

and

$$\cos\nu = \frac{x}{x_0\cosh\mu}, \quad \sin\nu = \frac{y}{x_0\sqrt{\cosh^2\mu - 1}}. \tag{A3}$$

Figure 1(b) shows that, as the coordinate μ grows, it represents increasingly large ellipses, all sharing the same foci, while ν varies from 0 to 2π along a whole turn around each ellipse. Thus, μ and ν define a sort of 'polar' coordinate system (respectively giving its 'modulus' and 'angle') with elliptic symmetry. The ellipse of $\mu = 0$ coincides with the segment $[-x_0, x_0]$. Over this degenerate ellipse, the coordinate ν is not uniquely defined.

Of particular interest for the applications in this paper are the distances d_+ and d_- from a point of coordinates (μ, ν) to the foci at $+x_0$ and $-x_0$, respectively. They are given by

$$d_\pm = \sqrt{(x \mp x_0)^2 + y^2} = x_0(\cosh\mu \mp \cos\nu). \tag{A4}$$

In turn, the surface element is

$$\mathrm{d}^2\mathbf{r} \equiv J\,\mathrm{d}\mu\,\mathrm{d}\nu = x_0^2(\cosh^2\mu - \cos^2\nu)\,\mathrm{d}\mu\,\mathrm{d}\nu. \tag{A5}$$

Remarkably, the Jacobian J coincides with the product of the distances to the two foci, $J = d_+d_-$. This coincidence is the origin of the substantial simplification of the integral in Equation (6) when expressed in elliptic coordinates.